Pergamon

1359-6454(95)00410-6

Acta mater. Vol. 44, No. 7, pp. 2581–2590, 1996

Published by Elsevier Science Ltd

1359-6454/96 $15.00 + 0.00

MICROBUCKLE PROPAGATION IN A UNIDIRECTIONAL CARBON FIBRE–EPOXY MATRIX COMPOSITE

S. SIVASHANKER, N. A. FLECK and M. P. F. SUTCLIFFE

Cambridge University Engineering Department, Trumpington Street, Cambridge CB2 1PZ, England

(Received 15 August 1995; in revised form 25 October 1995)

Abstract—Out-of-plane microbuckle growth is observed in a unidirectional carbon fibre–epoxy matrix composite under compressive loading. Experimental measurements of the overall kink-band width confirm that a growing microbuckle propagates in a crack-like manner rather than in a dislocation-like manner. The microbuckle is modelled as a bridged Mode I crack with compressive bridging tractions. A large scale bridging model with a crack tip toughness and a constant bridging stress is successful in correlating the length and width of a growing microbuckle with the remote stress. *Crown copyright © 1996*

1. INTRODUCTION

Carbon fibre–epoxy matrix composites are used in the automotive and aerospace industries to build light, strong structures with high fatigue resistance. They have also been identified as a suitable class of materials for use in naval and offshore structures where they can replace more conventional materials such as steel and aluminium. Their use eliminates the maintenance cost associated with corrosion protection required for metal structures in deep-water applications [1].

Long fibre–polymer matrix composites fail in tension by the random fracture and pull-out of fibres. Compressive failure is, typically, by the co-operative *kinking* of the fibres, see Fig. 1. During this kinking process the supporting matrix material deforms predominantly in shear and in a non-linear manner. Hence, the compressive failure mechanism is labelled *plastic kinking*. The term *microbuckling* is also used to describe this type of failure. The continuous fibre reinforcements in these composites are not aligned perfectly but possess local areas of waviness, typically of a few degrees in magnitude. It is from these regions of misalignment that kinking failure initiates.

In this paper we address some fundamental aspects of damage development in compression and deduce whether a growing microbuckle advances in the manner of a crack or of a dislocation. The investigation of kink-band propagation in fibrous polymer composites is difficult, since unstable propagation usually occurs as soon as kinking has initiated. Notched unidirectional T800/924C carbon fibre–epoxy composites typically split at the notch ends when loaded along the fibre direction. Sutcliffe and Fleck [2] overcame this problem and succeeded in encouraging stable microbuckle growth from a sharp centre-notch by having an additional vertical notch, cut in the fibre direction along the mid-plane of the centre-notch. In the present investigation we overcome this problem by first nucleating a microbuckle in unidirectional T800/924C carbon fibre–epoxy composite by denting the root of a starter notch. The specimen is then loaded in axial compression and stable microbuckle growth is observed in a consistent, repeatable manner for microbuckle lengths limited only by the ligament length of the specimen (35 mm for the geometry employed).

2. TEST METHOD

2.1. Specimen design

The material system consists of Toray T800 carbon fibres in Ciba Geigy 924C epoxy matrix. An edge-notch, 15 mm long and 3 mm wide, was machined in 50 mm wide specimens, and aluminium end tabs were bonded to the specimen ends using a hot cure epoxy adhesive to enable a smooth transfer of load. The specimen geometry is shown in Fig. 2. All specimens were of unidirectional lay-up and were nominally 3 mm thick.

A roller bearing of diameter 2 mm was used to indent the notch root while loading the specimens in three-point bending; the geometry of the loading rig is shown in the insert of Fig. 2. This indentation nucleated a microbuckle from the notch root with a length of about 2 mm. Kyriakides and Babcock [3] used a similar idea to investigate buckle propagation along long circular pipes subjected to an external pressure. In these tests they introduced a dent near one end of a long pipe to cause buckle formation and subsequently controlled its propagation via the rate of injection of the external pressurising fluid.

To aid measurement of microbuckle length, the region ahead of the notch on the front face of the test specimen was scribed at 2 mm intervals using a

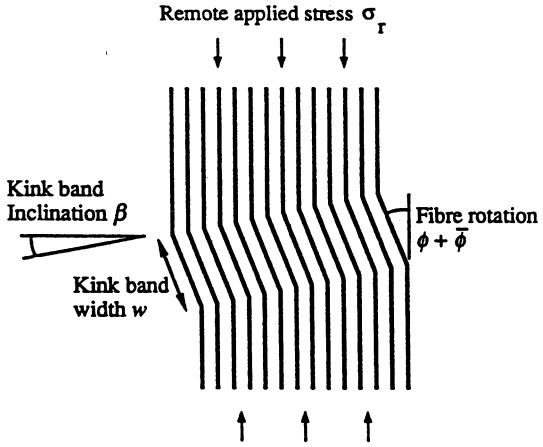

Fig. 1. Schematic of out-of-plane microbuckling in unidirectional composite under compressive loading.

diamond tool. These lines were then filled with white engraver's wax.

2.2. *Mechanical testing and examination*

The specimen was held in wedge grips and loaded in compression using a screw-driven test machine in displacement control. Anti-buckling guides lubricated with PTFE spray prevented Euler macro-buckling of the specimen. Special attention was given to specimen alignment between the lower and upper wedge grips.

During the test the region ahead of the notch root was video-recorded using a high magnification video camera. This enabled us to record the sequence of damage events. The initial loading rate was 0.01 mm/s. Upon the first sign of microbuckle growth the loading rate was reduced to 0.001 mm/s in order to view microbuckle propagation over an adequate time-scale.

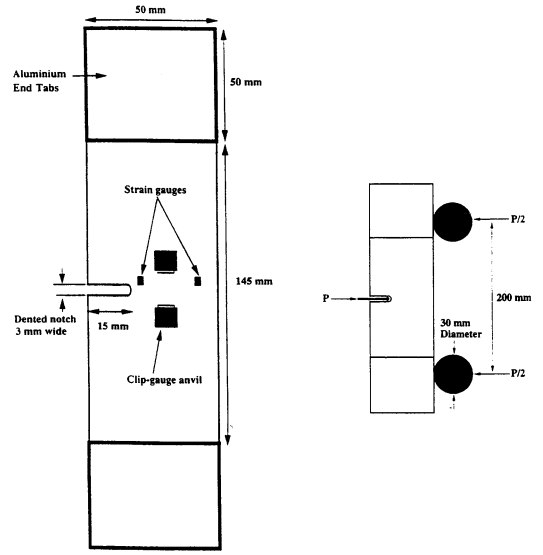

Fig. 2. Specimen geometry. The gauge length of the clip gauge is 10 mm. The insert of the figure shows the three-point bend loading arrangement used to nucleate a microbuckle.

Two experiments were conducted with this test set-up: experiment A and experiment B. For each experiment a single specimen was employed.

Experiment A. A microbuckle was nucleated by three point bend loading and propagated to about mid-way across the ligament of the specimen under axial loading. The test was then terminated and the detailed geometry of the microbuckle was determined by examining the side faces of the specimen in the Scanning Electron Microscope (SEM).

Experiment B. Foil strain-gauges were placed 1.5 mm above the expected trajectory of the microbuckle, using a specimen of geometry given in Fig. 2. One strain gauge was located 4 mm ahead of the notch tip and a second gauge was located 24 mm ahead of the notch tip. A clip gauge of gauge length 10 mm was located 14 mm ahead of the notch tip (see Fig. 2).

A microbuckle was nucleated by three-point bend loading, and upon application of axial loading the microbuckle was grown across the entire ligament of the specimen. The strain, load and clip-gauge readings were recorded every half second using a computerised data logger.

3. EXPERIMENTAL RESULTS AND OBSERVATIONS

3.1. *Out-of-plane microbuckling*

Visual observation of the specimens revealed that out-of-plane microbuckling occurred in both experiments A and B. Figure 3 shows a magnified view of the kink band which has propagated mid-way across the specimen ligament in experiment A. The arrested microbuckle extends 16 mm from the notch root, and the normal to the kink band is inclined at an angle of about 25° to the fibre direction. Examination of specimen A within the SEM revealed that the microbuckle behaves as a Mode I crack, such that the material above the microbuckle band slides over that below. The extent of this sliding reduces with decreasing distance from the microbuckle tip.

The specimen thickness of 3 mm is much less than the specimen ligament length of 35 mm. Hence there is much less constraint in the through-thickness direction and so out-of-plane microbuckling was expected in preference to in-plane microbuckling. Attempts to trigger in-plane microbuckling by clamping the specimens laterally with thick glass blocks were unsuccessful. In this paper we focus attention on modelling out-of-plane microbuckling which is believed to be the preferred failure mode.

3.2. *Microbuckle growth versus applied stress*

Microbuckle extension is shown as a function of remote stress σ_r in Fig. 4, for both experiments A and B. We note that microbuckle propagation begins

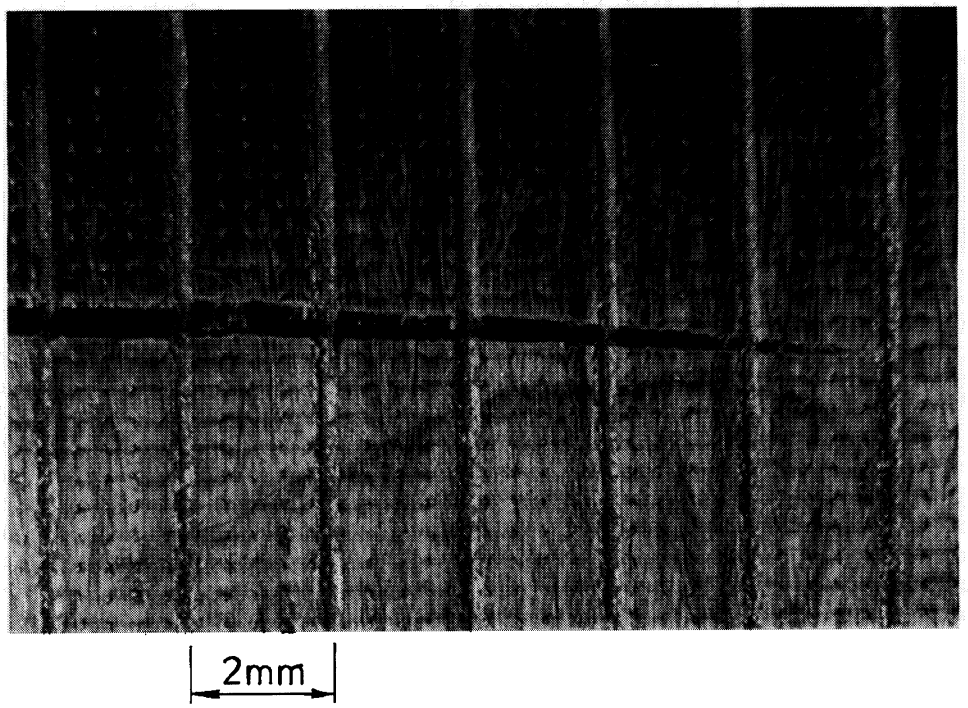

Fig. 3. Side view of specimen, showing the microbuckle tip at the completion of experiment A. The vertical scribed lines are 2 mm apart.

at $\sigma_r \approx 140$ MPa, and σ_r increases to a plateau value of about 180 MPa. The microbuckle grew at a speed which increased from 0.04 to 0.28 mm/s during the test.

3.3. *Measurements of local bridging stresses*

The bridging stresses across the growing microbuckle were measured using strain-gauges in experiment B. The results are shown as a function of time (during the test) in Fig. 5, and as a function of microbuckle tip location in Fig. 6. We note that the axial stress measured by each strain gauge attains a maximum when the microbuckle tip lies adjacent to the gauge. For the strain gauge placed 4 mm from the notch root, the bridging stress asymptotes to a constant value of about 100–133 MPa in magnitude when the microbuckle has advanced about 20 mm past the strain gauge. These values are in good agreement with the value of about 140 MPa reported by Sutcliffe and Fleck [2] using a different specimen geometry.

3.4. *Kink-band width measurements*

After completion of experiment A, the side faces of the specimen were examined in the scanning electron microscope. Multiple kink bands were observed, as illustrated in Fig. 7. Such multiple kink band formation has also been reported previously by Sutcliffe and Fleck [2]. The width of the overall kink band increases from about 70 μm at the microbuckle tip to about 800 μm at the notch root. This is illustrated in the sequence of micrographs

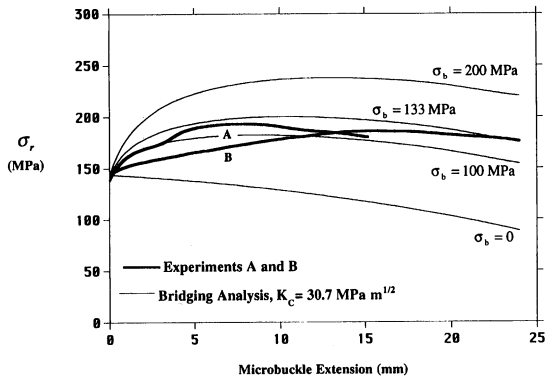

Fig. 4. Comparison of measured collapse response with predictions from the large-scale crack bridging model.

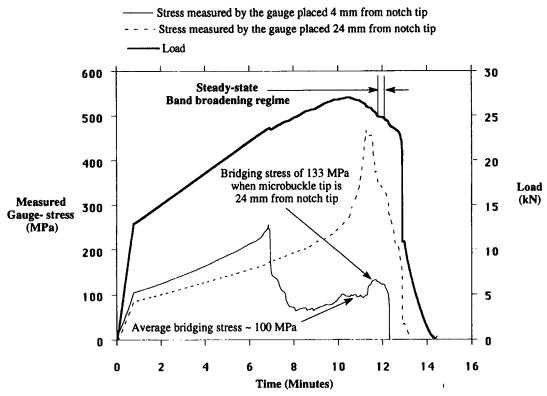

Fig. 5. Load and strain-gauge stress as a function of time in experiment B.

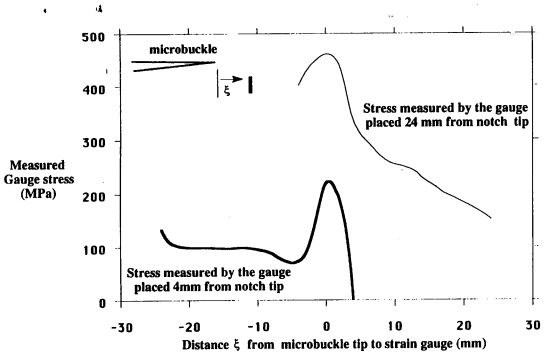

Fig. 6. Strain-gauge stress as a function of distance from the microbuckle tip to the strain gauge. Experiment B.

(Figs 7(a)–(d)) taken at a series of locations from the notch root to the microbuckle tip. The variation of microbuckle width along the length of the microbuckle is plotted in Fig. 8(a); the number of individual kink bands increases from a single band at the microbuckle tip to about six bands at the notch root (see Fig. 8(b)). The width of the individual kink bands is constant at about 100 μm (i.e. 20 fibre diameters), as shown in Fig. 8(c). This measured width of individual kink bands supports the predicted width of 15–20 fibre diameters by Fleck *et al.* [4].

3.5. Band broadening

It is clear from Figs 3 and 8(a) that a microbuckle advances in a crack-like manner, with broadening of the microbuckle behind its tip. The bridging stress across the faces of the microbuckle settles down to a constant value (see the gauge stress measured 4 mm from the notch root in Fig. 5). In experiment B, the microbuckle grew across the ligament of the specimen; the microbuckle then continued to broaden in the fibre direction under a constant applied stress (see Fig. 9.) Steady-state band broadening is superseded by the sliding-off of the two halves of the specimen along one of the kink band fracture planes. This is sketched in Fig. 9.

The phenomenon of steady-state band broadening has been reported previously by Moran *et al.* [5] for IM7 carbon fibre–PEEK composite. The IM7 fibres have sufficient strength to remain unbroken during microbuckling, and so multiple kink bands were not observed by Moran *et al.* [5]. In other respects, however, our findings are in agreement with theirs. Band broadening is an example of steady-state buckle propagation, whereby unbuckled fibres are convected into a buckled state under constant remote stress.

The observations described above show that kink bands propagate in a crack-like manner and not in a dislocation-mode. If microbuckle propagation were akin to a dislocation motion, we would expect to observe constant kink-band widths and a fixed value of shear displacement across the microbuckle. A dislocation mode of microbuckle propagation mode has been suggested in several past studies on kink-band propagation [6, 7].

4. THE LARGE-SCALE CRACK BRIDGING MODEL

In this section we describe the use of established fracture mechanics methods to correlate the experimentally observed collapse response. The approach is similar to that described in Refs [2] and [8], but the details of the implementation differ, as described below. A large-scale crack bridging model is employed on the basis that a microbuckle propagates in a crack-like manner. Accordingly, we treat the out-of-plane microbuckle as a bridged Mode I crack in compression. The crack is ascribed a tip toughness G_C and a constant normal bridging stress across its flanks. The microscopic origins of the tip toughness stem from the strain energy stored in the transition region between unbuckled and buckled fibres of the microbuckle. This is discussed in further detail by Fleck and Shu [9], and by Sutcliffe *et al.* [10]. The constant crack bridging stress is associated with the phenomenon of steady-state band broadening.

Although the specimen used in the current study is a single edge-notch specimen, we model it by both a single-edge notch and a centre-notch configuration. Under prescribed end loads, single edge-notch specimens rotate due to their asymmetrical geometry. In practice the clamping action of the wedge grips allows little rotation of the specimen ends. This resistance to end-rotation results in an end-moment which has to be taken into account in any full analysis of the single-edge notch specimens. We avoid the complication of this end-moment in our computation by treating the specimen geometry as being equivalent to one half of a centre-notch geometry, as shown in Fig. 10. Sutcliffe and Fleck [8] have verified experimentally that the effect of clamping a single-edge notch specimen is to make it behave like a half centre-notch specimen under uniform axial stress.

4.1. Calculations with a centre-notch configuration

For the single-edge notch geometry of Fig. 2, the initial notch depth a_0 equals 15 mm and the specimen width b equals 50 mm. A microbuckle of length l grows from the root of the notch (assumed sharp), driven by a remote applied stress σ_r. The specimen is mimicked by a rectangular panel of width $2b$ and initial notch length $2a_0$. The microbuckle is modelled by a crack of length l at the end of the notch, with a constant crack tip toughness G_c and a constant bridging stress of magnitude σ_b across the crack flanks.

The stress intensity factor at the crack tip due to the applied remote compressive stress σ_r is denoted as K_r and that due to the constant bridging stress along the microbuckle length σ_b is labelled K_b. The net stress intensity factor at the microbuckle tip K_t is

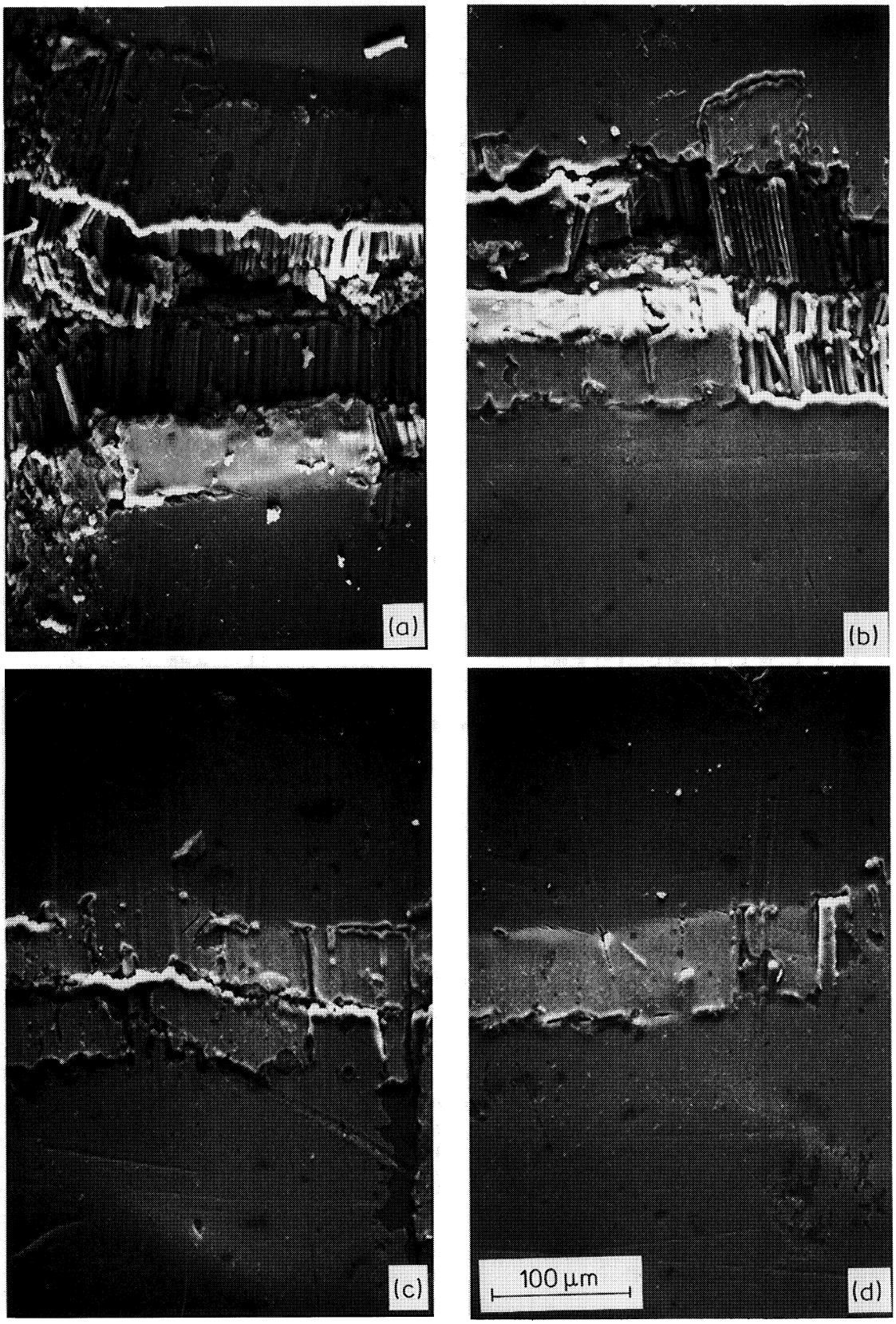

Fig. 7. Micrographs at various locations along the microbuckle in experiment A. The microbuckle tip extends 16 mm from the notch root. Loading is parallel to the fibre direction and the four micrographs have the same magnification. (a) Four kink bands at a location 8 mm behind the microbuckle tip; (b) three kink bands at a location 6 mm behind the microbuckle tip; (c) two kink bands at a location 3 mm behind the microbuckle tip; and (d) single kink band at a location 1 mm behind the microbuckle tip.

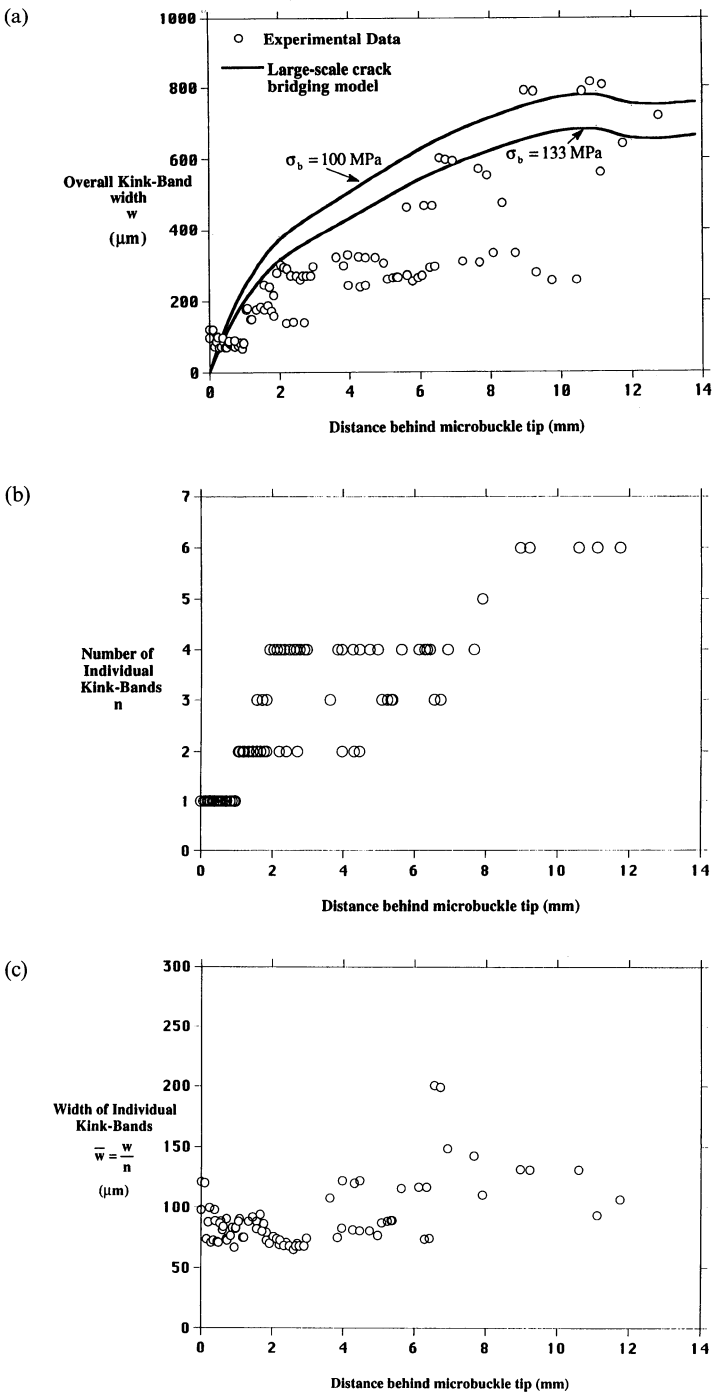

Fig. 8. (a) Width of overall microbuckle predicted by the large-scale crack bridging model. (b) Number of individual kink bands within the overall microbuckle as a function of distance from the microbuckle tip. (c) Width of individual kink bands within the overall microbuckle as a function of distance from the microbuckle tip.

given by superposition of the contributions from remote loading and bridging. Thus

$$K_t = K_r + K_b, \tag{1}$$

which can be re-written in the form

$$K_t = (F_r\sigma_r - F_b\sigma_b)\sqrt{\pi a}, \tag{2}$$

where $a = a_0 + l$ is the sum of the initial notch length and the microbuckle length. Detailed expressions for the functions F_r and F_b are given in the Appendix.

The applied stress σ_r is predicted as a function of the microbuckle length by equating the total crack tip stress intensity factor K_t to an assumed fracture

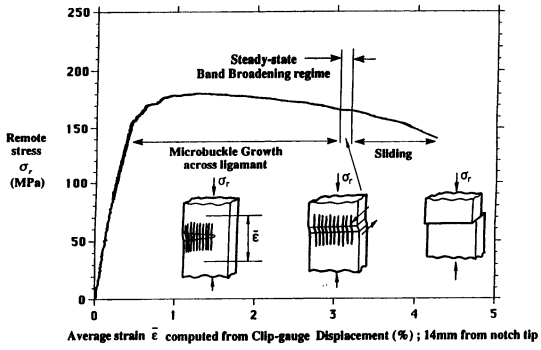

Fig. 9. Collapse response of the specimen in experiment B.

toughness K_C. The value of K_C is deduced from the measured load for microbuckle initiation.

An additional check on the accuracy of the crack model comes from comparing the predicted crack overlap displacement δ with the measured microbuckle width. The in-plane, mode-I crack overlap displacement δ is predicted from the remote loading and the crack bridging tractions by

$$\frac{\delta E'}{a} = U_r\sigma_r - U_b\sigma_b, \tag{3}$$

where the functions U_r and U_b are calculated using weight function theory (see the Appendix for details). The constant E' is the plane stress orthotropic modulus and appears in the standard formula [11]

$$G = \frac{K^2}{E'}. \tag{4}$$

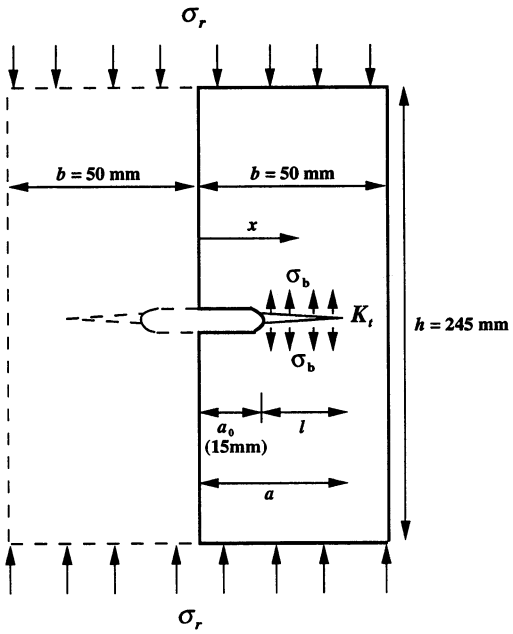

Fig. 10. Single-edge notch specimen analysed as half of a centre-notch geometry under uniform axial compression.

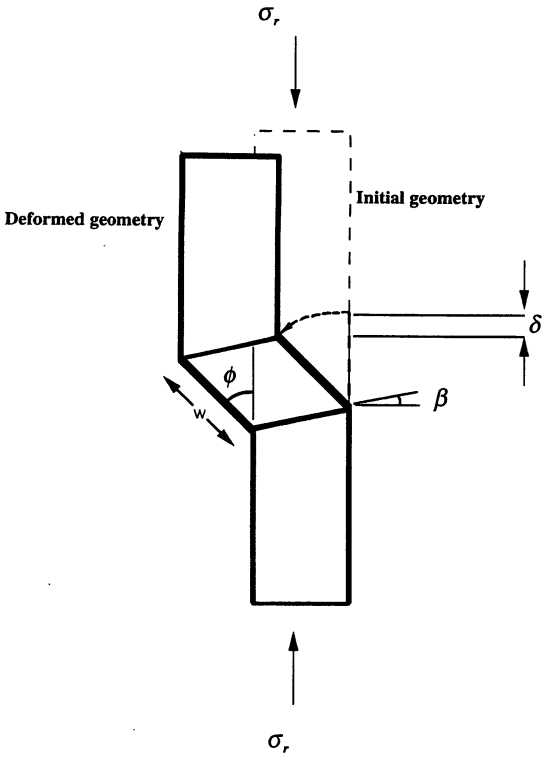

Fig. 11. Geometry of an out-of-plane microbuckle after the fibres in the band have rotated through an angle $\phi = 2\beta$ to the locked-up configuration.

Here, G is the Mode I strain energy release rate and K is the Mode I stress intensity factor. The usual expression for E' in terms of the orthotropic elastic constants is included in the Appendix for completeness.

We define the width w of a microbuckle band at any location by the fibre length contained within the microbuckle band. The crack overlap displacement δ represents the end-shortening associated with fibre rotation in the microbuckle band. In the microbuckled band, fibres rotate out-of-plane through an angle ϕ given by $\phi = 2\beta$, where β is the orientation of the microbuckle band, as shown in Fig. 11. The condition $\phi = 2\beta$ is a statement that fibres rotate until the volumetric strain in the band vanishes and then "lock-up" (see Fleck and Budiansky [6]). Making the assumption that the fibre rotation $\phi = 2\beta$ within the microbuckle band of width w, we can estimate the crack overlap displacement δ by using the straightforward kinematic expression

$$\delta = w(1 - \cos\phi) \tag{5}$$

as depicted in Fig. 11. Although experimental observations [2, 5] show that there is a short region at the tip of the microbuckle where the fibres have rotated by less than the lock-up angle 2β, equation (5) is applied to observations well outside this tip region.

4.2. Calculations with single-edge notch configuration

The calculations for single-edge notched configuration, assuming uniform remote applied stress (without end-moments) follows the same procedure as outlined above. Expressions for F_r, F_b, U_r and U_b are outlined in Tada *et al.* [12] and in Wu and Carlsson [13].

5. PREDICTIONS OF THE CRACK MODEL

In this section the predicted evolution of microbuckle length and width are compared with the observed response. The measured microbuckle-initiation stress of 140 MPa in both experiments A and B is used to deduce a crack tip fracture toughness of $K_C = 30.7$ MPa m$^{1/2}$; the corresponding tip toughness G_C equals 17.3 kJ/m^2, since $E' = 54.8$ GPa.

Predictions of the microbuckle length as a function of applied stress are given in Fig. 4, for a range of assumed values for the crack bridging stress σ_b. Recall that it was found experimentally that the local bridging stress, σ_b ranges from 100 to 133 MPa for the T800/924C unidirectional laminates (Figs 5 and 6). The measured collapse response (applied stress versus microbuckle length) in experiment A is bounded by the predictions for $\sigma_b = 100$ and 133 MPa (see Fig. 4). Agreement is less satisfactory for experiment B: although test parameters were nominally identical, specimen B was somewhat weaker than specimen A during the early stages of microbuckle propagation and the measured collapse response is below both predictions for $\sigma_b = 100$ and 133 MPa. Note that the predicted response is sensitive to the precise value of σ_b: the predicted collapse curve for $\sigma_b = 0$ lies much lower than the measured response. In contrast, an assumed value of $\sigma_b = 200$ MPa gives a much stronger response than that observed experimentally.

Calculations with a *single-edge notch configuration* require an assumed fracture toughness of 47.8 MPa m$^{1/2}$ and $\sigma_b = 340$ MPa to fit the experimental data (see Fig. 12). This higher bridging stress

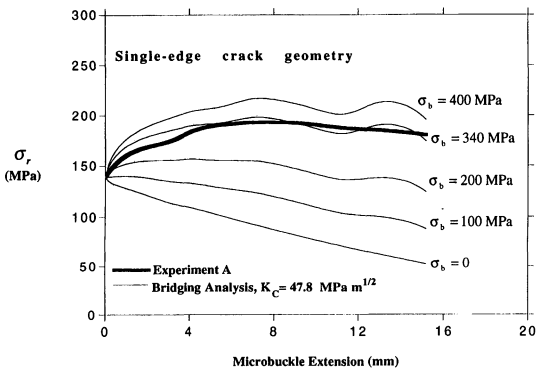

Fig. 12. Comparison of measured collapse response with the predictions of the large-scale crack bridging model for a single-edge crack geometry.

is not consistent with that observed experimentally via the strain gauge measurements (Figs 5 and 6). As discussed in the previous section, the grip condition in our tests was sufficiently constrained against end rotation that the usual edge-crack K-calibration is significantly in error and a centre-cracked geometry is more representative.

The predicted collapse response (applied stress versus microbuckle length) for the edge-cracked geometry matches the observed response only by taking unreasonable values for K_C and σ_b. This demonstrates the robustness of the large-scale crack bridging model. It also cautions us with regards to its pitfalls. The crack analyses of both configurations can model the experimentally observed variation of propagation stress with microbuckle growth with arbitrarily selected values of K_C and σ_b. It is clearly necessary to measure crack bridging tractions directly in order to make sensible deductions about the quality of a large scale bridging model.

To give further credence to the large-scale crack bridging model we compare the measured microbuckle width with predictions from the bridging analysis for the *centre-notch* configuration. Equation (5) is used to relate the overlap displacement δ to the measured width w of the microbuckle, taking the out-of-plane microbuckle to be inclined at the measured angle of $\beta = 25°$. The crack bridging model takes as input $K_C = 30.8$ MPa m$^{1/2}$, and σ_b lies in the range 100–133 MPa. It is clear from Fig. 8(a) that the crack theory adequately predicts the observed trend of increasing microbuckle width with distance behind the microbuckle tip.

The good agreement between the large-scale *crack* bridging model predictions and experimental observations support our claim that a growing microbuckle is a crack-like feature. Sutcliffe and Fleck [2] arrived at similar conclusions by measuring the overlap displacement δ in the wake of a growing microbuckle for T800/924C unidirectional laminates. They observed a continuous increase in overlap displacement at the notch root with microbuckle growth: this supported their treatment of the microbuckle as a compressive Mode I crack. They found good agreement between the calculated and measured overlap displacements by using a large-scale bridging model with an assumed value of σ_b of 220 MPa, and a tip toughness of 11 kJ/m^2. These values are in rough agreement with the measured values of $\sigma_b = 100$–133 MPa and $G_C = 17.3$ kJ/m^2 in the current study.

6. CONCLUSIONS

Experimental measurements of the overall kink-band width of an arrested microbuckle in unidirectional carbon fibre–epoxy laminates have confirmed that a growing microbuckle propagates in a crack-like manner. The overall microbuckle width increases from about 70 μm at the microbuckle tip to

about 800 μm near the notch root. During propagation, the microbuckle broadens by the formation of multiple kink bands. The preferred mode of microbuckle propagation in panels with thickness-to-width ratios much less than unity is by out-of-plane microbuckling. Out-of-plane microbuckling in this unidirectional material is modelled as a bridged compressive Mode I crack. A large scale bridging model with an inferred tip toughness and a constant bridging stress is successful in predicting the propagation stress and overall kink-band widths. For T800/924C carbon–epoxy laminates the measured tip toughness is $G_C = 17.3$ kJ/m^2 and the measured bridging stress is of the order of 100–133 MPa.

Acknowledgements—The authors are grateful to Dr P. T. Curtis of the Defence Research Agency, Farnborough and Dr Yapa D. S. Rajapakse (Office of Naval Research, U.S.A., grant number 0014-91-J-1916) for supporting this research. The Ph.D. sponsorship offered to one of the authors (S. S.) from the Nanyang Technological University of Singapore (NTU), School of Mechanical and Production Engineering is gratefully acknowledged. Thanks are also due to the Nuffield Foundation for financial support. The technical support from Messrs R. Brand, A. Heaver, R. Denston, S. Marshall, B. Butler and D. Miller is acknowledged with deep appreciation.

REFERENCES

1. M. M. Salama, *Proc. Offshore Technology Conference (OTC 5185)*, p. 297 (1986).
2. M. P. F. Sutcliffe and N. A. Fleck, *Acta metall. mater.* **42,** 2219 (1994).
3. S. Kyriakides and C. D. Babcock, *ASME J. Pressure Vessel Technol.* **103,** 328 (1981).
4. N. A. Fleck, L. Deng and B. Budiansky, *J. appl. Mech.* **62,** 329.
5. P. M. Moran, X. H. Liu and C. F. Shih, *Acta metall. mater.* **43,** 2943 (1995).
6. N. A. Fleck and B. Budiansky, *Proc. IUTAM Symp.* (edited by G. J. Dvorak), Troy, New York, 29 May–1 June. Springer-Verlag, Berlin (1990).
7. D. C. Lagoudas and A. M. Saleh, *J. Compos. Mater.* **27,** 83 (1993).
8. M. P. F. Sutcliffe and N. A. Fleck, *Int. J. Fract.* **59,** 115 (1993).
9. N. A. Fleck and J. Y. Shu, Manuscript in preparation (1996).
10. M. P. F. Sutcliffe, N. A. Fleck, X. J Xin, *Proc. R. Soc. London*. in press.
11. G. C. Sih, P. C. Paris and G. R. Irwin, *Int. J. Fract. Mech.* **1,** 189 (1965).
12. H. Tada, P. C. Paris and G. R. Irwin, *The Stress Analysis of Cracks Handbook*, 2nd edition. Paris Productions Inc, Paris (1985).
13. X. R. Wu and A. J. Carlsson, *Weight Functions and Stress Intensity Factor Solutions*. Pergamon Press, Oxford (1991).
14. Z. Suo, G. Bao, B. Fan and T. C. Wang, *Int. J. Solids Struct.* **28,** 235 (1991).
15. G. Bao, S. Ho, Z. Suo, and B. Fan, *Int. J. Solids Struct.* **29,** 1105 (1992).
16. A. C. Kaya and F. Erdogan, *Int. J. Fract.* **16,** 171 (1980).

†An error in the correction factor has been corrected via a private communication with Bao (1992).

APPENDIX

The plane stress orthotropic modulus E' in equation (4) can be computed from laminate properties such that

$$E' = \lambda^{1/4}\left\{\frac{(2E_1E_2)}{1+\rho}\right\}^{1/2}, \tag{A1}$$

where

$$\lambda = \frac{E_2}{E_1}$$

$$\rho = \frac{\sqrt{E_1E_2}}{2G_{12}} - (\nu_{21}\nu_{12})^{1/2}$$

$$\nu_{12} = \frac{E_1}{E_2}\nu_{21}. \tag{A2}$$

Subscripts 1 and 2 refer to directions perpendicular and parallel to the fibre direction, respectively. E is Young's modulus, G_{12} is the shear modulus and ν is the Poisson's ratio. The elastic constants λ and ρ are non-dimensional material parameters to characterise the degree of orthotropy [14]. For an isotropic material of Young's modulus E, $\rho = 1$, $\lambda = 1$ and $E' = E$.

Suo *et al.* [14] have developed an orthotropy rescaling technique whereby isotropic solutions may be used as an approximation for orthotropic materials provided certain conditions are satisfied. The technique rescales the geometry and boundary conditions of the original orthotropic problem with a function of λ; this transforms the problem to an equivalent isotropic one, for which established solutions exist. Using this technique Bao *et al.* [15] have catalogued the stress intensity factors of various notched unidirectional specimens. With materials for which $\rho = 1$, the functions F_r, F_b, U_r and U_b (using weight function analysis) could have been used immediately, but for T800/924C unidirectional composites, λ and ρ are 17.4 and 3.1, respectively. Therefore a correction for orthotropy is required.

Bao *et al.* [15] have demonstrated through finite element analysis that the effect of λ is negligible for a sufficiently long and narrow specimen. They found that the stress intensity factors of notched specimens approach their isotropic value when $\lambda^{1/4}h/2b \geqslant 2.0$. With $h = 245$ mm and $b = 50$ mm for the current specimen geometry, this requirement is more than satisfied (see Fig. 10). The ρ dependence is taken into account by applying a multiplicative correction factor† $Y(\rho)$ to the K calibration for both centre-notched and single-edge notched configurations [15]:

$$Y(\rho) = (1 + 0.1(\rho - 1) - 0.016(\rho - 1)^2 + 0.002(\rho - 1)^3)\left(\frac{2}{1+\rho}\right)^{1/4}. \tag{A3}$$

Most of the calculations in this section are adopted from the text by Wu and Carlsson [13] and Tada *et al.* [15]. Suitable corrections for the effect of orthotropy are included. Consider first the centre-cracked panel shown in Fig. 10 with initial notch length a_0 and microbuckle length l. The combined length of the microbuckle and initial notch is $a = a_0 + l$. The expression for F_r is obtained from Ref. [12] with the correction term $Y(\rho)$ included

$$F_r(A) = Y(\rho)\{1 - 0.025A^2 + 0.06A^4\}\sqrt{\sec\frac{\pi}{2}A}, \tag{A4}$$

where $A = a/b$ (see Fig. 10). For $\rho = 3.1$, equation (A3) gives a 4% correction which we take into account in computing F_r and F_b.

The expression for F_b is obtained using the weight function method of computing stress intensity factors (see Wu and Carlsson [13]). For a centre-notched configuration in a finite plate with uniform crack face loading along the faces of the microbuckle, the function F_b is given by

$$F_b(A) = \frac{Y(\rho)}{\pi}\sum_{i=1}^{3}\beta_i(A)Q_i(A_0/A), \tag{A5}$$

where $A_0 = a_0/b$, and

$$Q_1(Z) = \cos^{-1}(Z) \tag{A6}$$

$$Q_i(Z) = \frac{1}{2i-2}\{(2i-3)Q_{i-1}(Z) - Z[1-Z^2]^{i-3/2}\} \text{ for } i \geqslant 2.$$

The functions β_i are tabulated by Wu and Carlsson [13].

The isotropic versions of the functions U_r and U_b are calculated using the weight function, method by integrating the product of the functions F_r and F_b with the weight function, respectively (Wu and Carlsson [13]). These expressions are

$$U_r(A, X/A) = \frac{1}{A_0}\int_0^{\mathcal{L}} \{1 - 0.025S^2 + 0.06S^4\} \times \sqrt{\sec\frac{\pi}{2}S}\sum_{i=1}^{3}\beta_i(S)[1-(X/S)^2]^{i-3/2}\,dS \tag{A7}$$

and

$$U_b(A, A_0/A, X/A) = \frac{1}{A_0\pi}\int_{A_0}^{A}\sum_{i=1}^{3}\beta_i(S)Q_i(A_0/S) \times \sum_{i=1}^{3}\beta_i(S)[1-(X/S)^2]^{i-3/2}\,dS, \tag{A8}$$

where $X = x/b$ is the dimensionless distance from the centre-line of the centre-notched specimen to the position where the displacement is to be calculated. The functions Q_i are again given by equation (A6).

Correction factors for the crack opening displacement are not given by Bao *et al.* [15]. However, Kaya and Erdogan [16] have calculated the crack opening displacements for orthotropic single-edge notch specimens under a uniform remote tension stress. Their results suggest that U_r and U_b should be decreased by 6% to allow for the effect of orthotropy. This small correction factor was included in our calculations.